CERN-ACC-2015-0055

hugo.bajas@cern.ch

Quench Analysis of High Current Density Nb3Sn Conductors in Racetrack Coil Configuration

H. Bajas, M. Bajko, B. Bordini, L. Bottura, S.Izquierdo Bermudez, J. Feuvrier, A. Chiuchiolo, J.C. Perez, G. Willering
CERN, Geneva, Switzerland

Keywords: Superconducting coils, Niobium-tin, analytical model

Abstract

The luminosity upgrade of the Large Hadron Collider (HL-LHC) requires the development of new type of superconducting cables based on advanced Nb_3Sn strands. In the framework of the FP7 European project EUCARD the cables foreseen for the HL-LHC project have been tested recently in a simplified racetrack coil configuration, the so-called Short Model Coil (SMC).
In 2013 to 2014, two SMCs wound with 40-strand (RRP 108/127) cables, with different heat treatment processes, reached during training at 1.9 K a current and peak magnetic field of 15.9 kA, 13.9T,and 14.3 kA, 12.7 Trespectively. Using the measured signals from the voltage taps, the behavior of the quenches is analyzed in terms of transverse and longitudinal propagation velocity and hot spot temperature. These measurements are compared with both analytical and numerical calculations from adiabatic models.The coherence of the results from the presented independent methods helps in estimating the relevance of the material properties and the adiabatic assumption for impregnated Nb_3Sn conductor modelling.

Presented at: ASC 2014, 10-15 August, Charlotte, USA

Geneva, Switzerland
June 2015

Quench Analysis of High Current Density Nb_3Sn Conductors in Racetrack Coil Configuration

H. Bajas, M. Bajko, B. Bordini, L. Bottura, S. Izquierdo Bermudez, J. Feuvrier, A. Chiuchiolo, J.C. Perez, G. Willering

***Abstract*— The luminosity upgrade of the Large Hadron Collider (HL-LHC) requires the development of new type of superconducting cables based on advanced Nb_3Sn strands. In the framework of the FP7 European project EUCARD the cables foreseen for the HL-LHC project have been tested recently in a simplified racetrack coil configuration, the so-called Short Model Coil (SMC). In 2013 to 2014, two SMCs wound with 40-strand (RRP 108/127) cables, with different heat treatment processes, reached during training at 1.9 K a current and peak magnetic field of 15.9 kA, 13.9 T, and 14.3 kA, 12.7 T respectively. Using the measured signals from the voltage taps, the behavior of the quenches is analyzed in terms of transverse and longitudinal propagation velocity and hot spot temperature. These measurements are compared with both analytical and numerical calculations from adiabatic models. The coherence of the results from the presented independent methods helps in estimating the relevance of the material properties and the adiabatic assumption for impregnated Nb_3Sn conductor modelling.**

***Index Terms*—Superconducting coils, Niobium-tin, analytical model**

I. INTRODUCTION

IN 2013 and 2014, two 40-strand Rod Restack Process (RRP) Rutherford cables, foreseen to be the conductor of the 11-T dipole for the LHC High Luminosity upgrade [1], have been tested at CERN in the one meter long Short Model Coil (SMC) magnet [2-5]. The RRP conductors differ in terms of insulation scheme (3*76 µm S2 or 76 µm S2 + 152 µm Mica) and heat treatment process [5-7]. It has been modified to improve the conductor stability by increasing the RRR from 90 to 130. The conductor short sample limit (I_{ss}) slightly decreased by 1.2% [4, 5]. Their performance and study of the thermodynamic behavior of impregnated Nb_3Sn conductor during a quench is of particular interest for the design and the protection of future larger scale magnets [1]. With SMC11T-1 and SMC11T-2 assemblies, the conductor critical currents have been measured as well as the transverse and longitudinal Quench Propagation Velocity (QPV). During both tests, the Hot Spot Temperature (HST) reached during the quench has been increased controlling the delay set between the quench detection and the current extraction. These measurements are valuable information for future quench detection system of less instrumented but longer magnets [8].

Manuscript received July 23, 2014.
H. Bajas is with CERN, Department of Technology, MSC group, CH-1211 Genève 23, Switzerland; phone: +41 22 766 2487; e-mail: hugues.bajas@cern.ch.
M. Bajko, B. Bordini, L. Bottura, S. Izquierdo Bermudez, J. Feuvrier, A. Chiuchiolo, J.C. Perez, G. Willering are with CERN, Department of Technology, MSC group, CH-1211 Genève 23, Switzerland.

As detailed in [4], SMC11T-1 quench current reached a plateau at 99% of I_{ss} at 4.3 K and a maximum current at 94% of I_{ss} at 1.9 K. However, instable current quenches occurred at 1.9 K with variations up to 1000 A from quench to quench. SMC11T-2 reached 97% of I_{ss} at 4.3 K and a maximum current at 89% at 1.9 K. Instable currents still occurred at 1.9 K but also now at 4.3 K and so despite the higher RRR. The current variations, around 200 A, were nonetheless lower than for SMC11T-1. Section II discusses about the occurrence of voltage spikes measured few milliseconds before instable quenches and their origin.
For both assemblies, the training quenches were located in the high field region of the coil, between the taps situated at the cable's straight parts of the pole turn. It allows the QPV to be assessed either with the time of flight or the voltage derivative methods. Section III presents the results from both methods compared to other numerical simulations [9].

During SMC11T tests, the temperature locally reached by the quenched conductor has been increased up to 220 K. As presented in section IV, three independent methods are used to compute the HST combining the measured local voltages and transport current in different ways. These semi-analytical approaches are introduced along with a sensitivity analysis to the main parameters and a comparison for all the quenches.

II. QUENCH CURRENT INSTABILITIES

For the instable quenches of both SMC-11T assemblies, the signals from the voltage taps that monitor the second and third turns around the pole, display voltage spikes few milliseconds before the normal transition. Fig 1 shows an example of precursor typically observed during the instable quenches. However, no such spike is observed for the training quenches when the quench current increases, or for the plateau quenches [4]. Their occurrence depends on the temperature and on the assembly and are symptomatic of erratic quench current.

With SMC11T-1, no precursor is detected during the training or plateau quenches at 4.3 K and 1.9 K. The quench location changes segments of the highest field zones (first three turns). For the instable quenches at 1.9 K, voltage spikes are detected at the taps U3-U4 (L4-L5) of the second and third turns, between 0.25 and 5 ms before the quench. Their amplitudes range from 50 to 250 mV. For SMC11T-2 instable current quenches, precursors of same amplitude are observed but now both at 4.3 K and 1.9 K. No precursor is observed for training or plateau quenches at both temperatures. For both magnets, the highest current is always obtained when quenches initiate at a point somewhere around the coil first turn without any precursors.

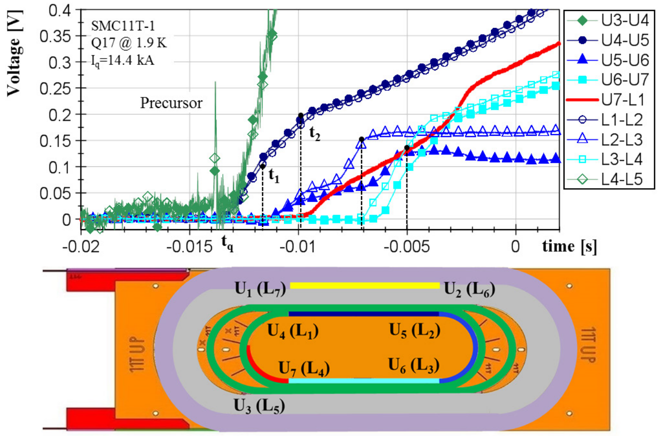

Fig. 1. Typical voltages during instable quench. 250 mV spike detected at the 2nd or 3rd turns. Transverse and longitudinal propagation from the middle of the straight section at time t_q toward the pole turn at t_1 and layer jump at t_2.

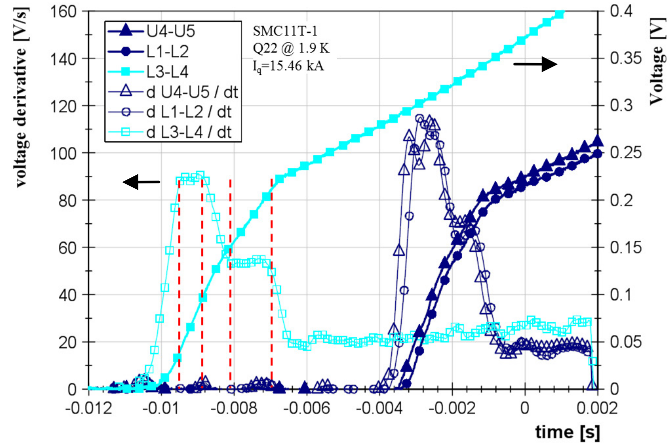

Fig. 2. Resistive voltages (hollow) and derivatives (full) for three segments. The red lines indicate the linear part of the voltage raise with corresponding plateau of the derivative. These values are used to estimate the QPV.

As discussed in [10-12], the effect of a small perturbation in RRP strands is more likely to provoke a normal transition at 1.9 K than at 4.3 K. This sensitivity also depends on the local RRR value. For both assemblies, the lowest performances at 1.9 K cannot be explained by critical current limits since higher Lorentz force can be reached at 4.3 K and since the temperature margin is higher at 1.9 K. The correlation between precursor occurrence and instable current seems rather to indicate that a perturbation of sufficient energy indeed triggers the transition. Despite of higher RRR for SMC11T-2, instability persisted. However, it cannot be excluded that the presence of Mica sheet in the insulation and the possible variation of the local mechanical stress applied to the coils (friction) influence the amplitude of the perturbations and thus the quench currents reached by both assemblies.

III. Quench Propagation Velocity

Most of the natural (not provoked) quenches initiate at the second and third turns of both layers. Some 0.1 to 5 ms after, the quench is detected between the voltage taps at the first turns of one side of the pole. A transverse propagation velocity is observed at 0.1 to 3 m/s for 300 microns of turn insulation. The quench starts at time t_q between U4 (L1) and U5 (L2). The first front crosses the first tap (U4, L1) at time t_1 when the slope of the voltage halves and the second front touches the second tap (U5, L2) at time t_2. The quench is then fully propagated and the voltage increases only due to the temperature. As visible in Fig.1, the quench propagates all around the pole in 11 ms. The heat from the second turn may contribute to the longitudinal quench propagation occurring at the first turn segments.

A. *Time of flight method*

For a quench initiating between the taps of the straight parts, U4 (L1) and U5 (L2), the longitudinal QPV is defined as the distance D between the taps divided by the time needed by both fronts to pass the voltage taps. The QPV is computed as:

$$v = \frac{D}{(t_1 - t_q) + (t_2 - t_q)}. \quad (1)$$

B. *Voltage derivative method*

During a quench, the measured voltage u [V] is composed of an inductive u_i and a resistive u_r voltages that writes:

$$u(t) = u_i + u_r = -L(t)\frac{dI(t)}{dt} + R(t)I(t). \quad (2)$$

L [H] stands for the inductance, I [A] for the current and R [Ω] for the ohmic resistance. The straight segments inductance L was measured to 0.4-0.6 μH. With the resistivity ρ [Ωm], the copper area S_{Cu} [m^2] and the quench length l [m], u_r writes:

$$u_r(t) = u(t) + L(t)\frac{dI(t)}{dt} = \frac{\rho(t)\, l(t)}{S_{Cu}} I(t). \quad (3)$$

The partial derivative of u_r along the time writes as follows:

$$\frac{du_r}{dt} = \frac{1}{S_{Cu}}\left(\frac{\partial u_r}{\partial \rho}\frac{d\rho}{dt} + \frac{\partial u_r}{\partial l}\frac{dl}{dt} + \frac{\partial u_r}{\partial I}\frac{dI}{dt}\right). \quad (4)$$

For the experimental signals, one can assume constant current and linear variation with time of u_r and ρ, thus:

$$I(t) = I_q\,, \frac{dI}{dt} = 0. \quad (5)$$

$$\rho(t) = a(t - t_q) + \rho_0 \quad \text{and} \quad \frac{d\rho}{dt} = a \quad (6)$$

$$u_r(t) = \alpha(t - t_q) \quad \text{and} \quad \frac{du_r}{dt} = \alpha. \quad (7)$$

$$l(t) = 2v(t - t_q) \quad \text{and} \quad \frac{dl}{dt} = 2v. \quad (8)$$

For the derivative method, the QPV is then computed as:

$$v = \frac{S_{cu}}{4I_q}\frac{\alpha}{a(t - t_q) + \rho_0}. \quad (9)$$

The parameter α [Vs^{-1}] is given by the first slope of u_r after t_q whereas a [Ωms^{-1}] and ρ_0 [Ωm] are identified on $\rho(t)$ after t_2. From Fig. 2, α = 90 Vs^{-1}, a = 10^{-7} Ωm.s^{-1} and ρ_0 = 5 10^{-10} Ωm.

Fig. 3 displays the QPV computed with both methods as function of the copper current density j_{cu} [A/mm^2]. The discrepancy comes from the origin of the quench (instable or plateau), the quench location (upper/lower layer, left/right segment), different positioning of the voltage taps during their setting up. The estimates from numerical models are in line with the data set [9]. The derivative method yields to lower velocities in general. At equal current, the velocities are basically higher for SMC11T-2 likely due to higher RRR and different insulation scheme.

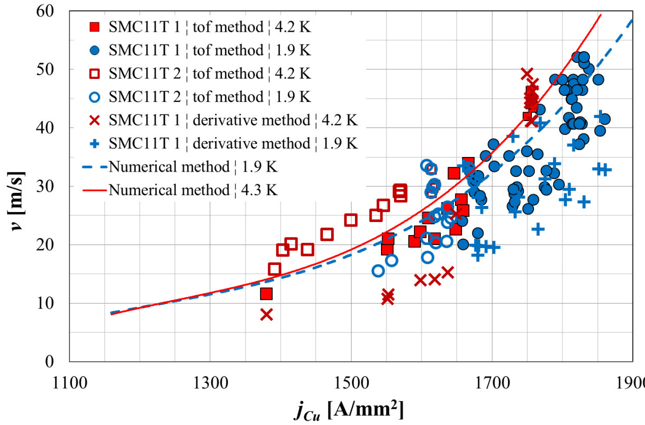

Fig. 3. Longitudinal QPV using the time of flight and the voltage derivative methods as function of j_{cu} for both RRP cables at 4.3 K and 1.9 K (marker). The results from numerical simulation [7] are also displayed (lines).

Fig. 4 shows the current profiles of all SMC11T quenches and Fig. 5 the deduced resistivities of the straight segments for both sides of both layers. These are used in the next section.

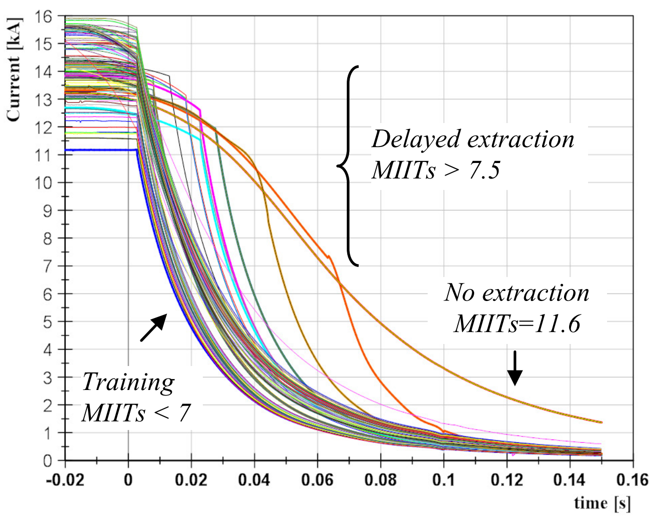

Fig. 4. Current profiles of the 225 quenches (training and higher deposited energy quenches). Controlling the delay of extraction, the deposited energy (*MIITs*) increases along with the hot spot temperature. The supplied current drops dramatically due to the magnet resistance growth.

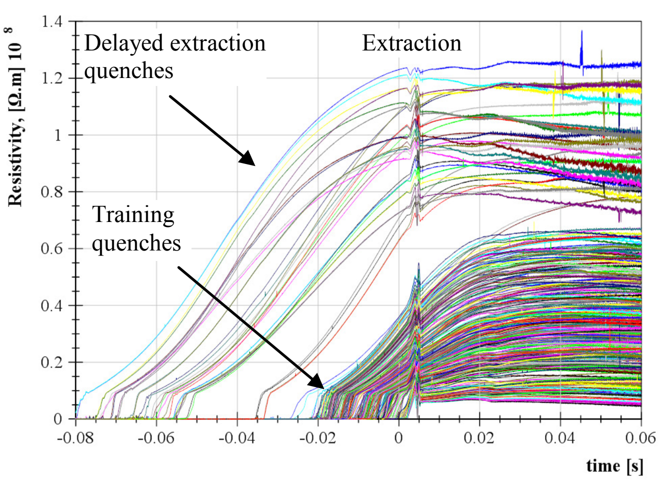

Fig. 5. Straight segment resistivities computed according to equation 3 during the quenches of SMC11T-1. The resistivity during propagation helps for the QPV assessment. Its identification allows deducing the segment temperatures.

IV. Hot Spot Temperature Assessments

During the quench, the temperature of the straight segment at the high field zone has been raised up from 60 K to 220 K by controlling the extraction delay. For the training quenches, a minimum delay of 12 ms was used (quench validation and the switch opening). With gradual increase the highest temperature is obtained without extraction (self-protected). The temperature of the four segments U4-5 (L1-L2) and U6-U7 (L3-L4) can be derived from the measured current and voltage signals and using the temperature dependence of the materials copper resistivity and Volumetric Heat Capacity (VHC) [$J.m^{-3}.K^{-1}$] [13, 14]. Three possible combinations of these parameters lead to complementary estimates of the HST as function of the deposited energy as these are now presented.

A. Material properties constitutive laws

The cable is a composite material formed by the conductor (superconductor, Nb_3Sn and copper stabilizer, Cu) and by the impregnated S2-glass insulation (G10). The VHC of Cu and Nb_3Sn depend on T [K], the material density ρ_v [$kg.m^{-3}$] and the heat capacity Cp_{300} [$Jkg^{-1}K^{-1}$] taken at 300 K.

$$VHC_{Cu,Nb_3Sn} = \rho_v \left(\frac{Cp_{300}}{1 + Cp_{300} / (\beta T^3 + \gamma T)} \right). \tag{10}$$

The VHC of *G10* is fitted by a logarithmic polynomial function of the temperature as:

$$VHC_{G10} = \rho_v \, 10^{\sum_{i=1}^{7} a_i \log T^i} . \tag{11}$$

The mixture law is used to derive the overall *VHC* of the composite using the respective material volume ratios ν:

$$VHC = \nu_{Cu} VHC_{Cu} + \nu_{Nb_3Sn} VHC_{Nb_3Sn} + \nu_{G10} VHC_{G10} \tag{12}$$

The theoretical resistivity ρ_{th} depends on the temperature, the Residual Resistivity Ratio *RRR* and the magnetic field *B* [T]:

$$\rho_{th} = \frac{C_0}{RRR} + m_r B + \left(\frac{C_1}{T^5} + \frac{C_2}{T^3} + \frac{C_3}{T} \right). \tag{13}$$

RRR is measured during the cooling and the warming of the magnet and range from 98 to 130 [4]. The coefficients C_i are: C_0=1.7, C_1=2.33 10^9, C_2=9.57 10^5 and C_3=160.

The magneto resistivity parameter m_r equals to 0.005 $\Omega m.T^{-1}$. *B* is given by the load-line with c = 0.75 T/A and d = 1.6 T as:

$$B(t) = c\, I(t) + d\,. \tag{14}$$

The numerical values of the parameters of the model are shown in Table 1 where *S* is the total area of the material.

TABLE I
Geometry and Material Properties Parameters

		OFHC Cu	Nb_3Sn	G10			
S	[mm^2]	8.55	6.84	9.15			
ρ_v	[kg/m^3]	8960	8040	1900			
Cp_{300}	[J/K/kg]	385	210	a_0	-2.41	a_4	-4.24
γ	[$J/K^2/kg$]	0.011	0.1	a_1	7.6	a_5	1.43
β	[$J/K^4/kg$]	0.0011	0.001	a_2	-8.3	a_6	-0.24
				a_3	7.33	a_7	0.02

B. Three semi-analytical methods of the hot spot temperature

The first method is based on the copper resistivity from which the temperature can be retrieved based on the inversion of equation (13) that can be written:

$$\text{Method 1}: \quad T(t) = \Phi\left(\rho_{\exp}(t) - \frac{C_0}{RRR} - m_r\, B(t)\right). \tag{15}$$

Φ is the identified inverse function of the temperature function and $\rho_{\exp}$ is the measured resistivity from (3).

The second and third methods are based on the energy balance between the generated and the stored energies in adiabatic condition. The energy E_{st} [J] stored between initial and final temperature is:

$$E_{st} = \int_{T_i}^{T_f} D\, S_t\, VHC_{composite}(T)\, dT. \tag{17}$$

The deposited energy E_d [J] is computed by either the square of the current I and the theoretical resistivity ρ_{th} or the product of the resistive voltage u_r by the current I as:

$$E_{d,1} = \int_{t_q}^{+\infty} \frac{\rho_{th} D}{S_{cu}} I^2\, dt \text{ and } E_{d,2} = \int_{t_q}^{+\infty} u_r I\, dt. \tag{16}$$

Where S_{cu} and S_t [m^2] are the copper and total conductor cross sections. Equaling E_{st} and both E_d, two independent temperature estimates can be done by first order numerical integrations of both separated variables equations. With the time increment Δt at step n, the temperatures as function of time can be written as:

$$\text{Method 2}: \quad T_n = T_{n\text{-}1} + \frac{\rho_{th}(T_{n\text{-}1}, B_{n\text{-}1}, RRR)\, I_{n\text{-}1}^2 . \Delta t_{n-1}}{S_{cu} S_t . VHC(T_{n\text{-}1})}. \tag{18}$$

$$\text{Method 3}: \quad T_n = T_{n\text{-}1} + \frac{u_{r\,n\text{-}1}\, I_{n\text{-}1}\, \Delta t_{n-1}}{D\, S_t\, VHC(T_{n\text{-}1})}. \tag{19}$$

The initial temperature has rather small impact on the results and is equal to 18.5 K. The application of equations 15, 18 and 19 to the signals of the quench without extraction is depicted in Fig. 6. The three estimates are similar within 20 K. The effect of G10 is visible as its contribution limit the temperature as part of the deposited energy is used to heat the insulation and impregnation. It seems that the impregnation should be taken into account as the curves get closer to the copper resistivity method which is independent of G10.

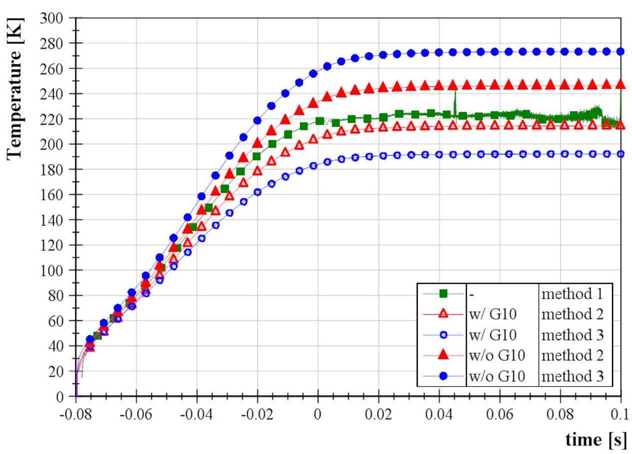

Fig. 6. Temperature evolution during a quench without extraction using three different combinations of the measured voltage and current. The insulation and impregnation (G10) is taking into account or not showing its contribution to the heat transfer. The first method is independent of G10.

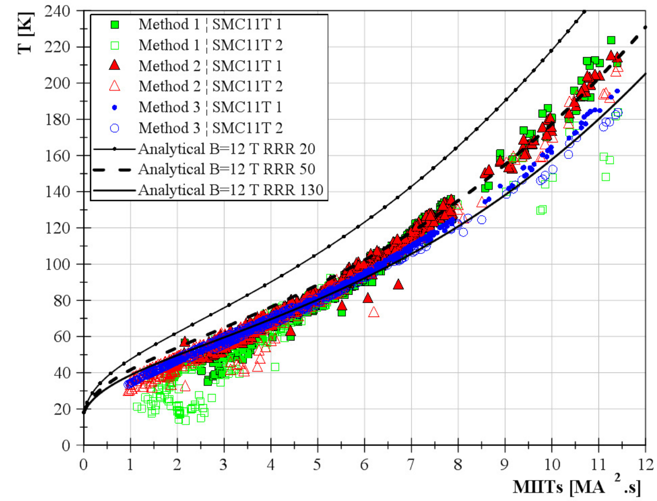

Fig. 7. HST during the 225 quenches using three different combinations of the measured voltages and current as function of MIITs. Expectation from theoretical calculation is in line with the data point depending on the RRR.

C. Hot Spot Temperature

For the following analysis, the Joule heating is represented by the integral of the square of the current I over the time t, here named *MIITs* [MA^2.s].

$$MIITs = \int_{t_q}^{+\infty} I^2\, dt. \tag{20}$$

In Fig. 7, the maximum temperatures computed by the three methods for the four segments are plotted as function of *MIITs* for all the quenches of SMC11T-1 and 2 test runs. The results form a coherent trend within 10 K variation showing the relevance of the material properties and of the computation methods. The reproducibility of the quench pattern leads to consistent temperature estimates for both sides of both layers. As expected, SMC11T-2 with higher RRR shows lower temperature. This temperature data are used to validate more elaborated models as [9, 14].

It is to be noted that, the conductor could not be tested at higher *MIITs* because of the fast magnet resistance growth that causes large drop of the supplied current (Fig. 4). Removing the extraction completely was not sufficient to reach temperature above 225 K. To be able to explore higher temperatures, a spot heater will be implemented in next SMC.

V. Conclusion

Two 11T dipole type conductors have been characterized in SMC assemblies in terms of quench performance, quench propagation velocity and hot spot temperature. The quench current instabilities observed in both assemblies have been related to voltage spike occurrence detected before the quench. In particular, no precursor is detected for plateau quenches. The longitudinal and transverse quench propagations have been measured. Assessment of the hot spot temperature using semi-analytical models has been presented. The analysis of the 225 quenches of SMC11T-1 and 2 tests shows good agreement with expectation from theory. It is important to note that no performance degradation was observed after the highest temperature quenches.

References

[1] M. Karppinen *et al.*, "Design of 11 T Twin-Aperture Nb_3Sn Dipole Demonstrator Magnet for LHC Upgrades", *IEEE Trans. Appl. Supercond.*, vol. 22, 4901504, 2012.

[2] J.C. Perez *et al.*, "The Short Model Coil (SMC) Dipole: An R&D Program Towards Nb_3Sn Accelerator Magnets", *IEEE Trans. Appl. Supercond.* vol. 22, 4002704, 2012.

[3] C. Kokkinos *et al.*, "The SMC (Short Model Coil) Nb_3Sn Program: FE Analysis With 3D Modeling", *IEEE Trans. Appl. Supercond.*, vol. 22 4900705, 2012.

[4] J. C. Perez *et al.*, The Short Model Coil (SMC) dipole performance using the 11T dipole type Nb_3Sn conductor, *IEEE Trans. Appl. Supercond.,* 2014.

[5] E. Fornassiere *et al.*, Status of the Activities on the Nb_3Sn Dipole SMC and of the Design of the RMC", *IEEE Trans. Appl. Supercond.* vol. 23, No. 3, 2013.

[6] AGY Advanced Materials, http://www.agy.com/products/s-glass/.

[7] Cogeby Excellence in Mica, http://www.cogebi.com/high-voltage-products.

[8] E. Todesco, "Quench limits in the next generation of magnets," *CERN Yellow Report 2013-006* 10-16(2013).

[9] S. Izquierdo Bermudez, H. Bajas, L. Bottura, "Quench Modeling in High-Field Nb_3Sn Accelerator Magnets," *Physics Procedia*, 2014.

[10] D. R. Dietderich et al, "Correlation Between Strand Stability and Magnet Performance," *IEEE Trans. Appl. Supercond.*, vol.15 , No. 2, pp. 1524, June 2005.

[11] B. Bordini, E. Barzi, S. Feher, L. Rossi, and A. V. Zlobin, "Self-field effects in magneto-thermal instabilities for Nb-Sn strands," *IEEE Trans. Appl. Supercond.*, vol. 18, pp. 1309–1312, 2008.

[12] Arup K. Ghosh, "Effect of Copper Resistivity and Filament Size on the Self-Field Instability of High-Jc Nb3Sn Strands," *IEEE Trans. Appl. Supercond.*, vol. 23, No. 3, pp. 7100407, June 2013.

[13] G. Manfreda, "Review of ROXIE's Material Properties Database for Quench Simulation," *CERN internal note 2011-24*, EDMS 1178007.

[14] P. Ferracin et al., "Thermal, Electrical and Mechanical Response to a Quench in Nb_3Sn Superconducting Coils", *IEEE Trans. Appl. Supercond.*, vol. 14, No.2, June 2004